*Antibody Therapeutics*, 2025, tbaf006
https://doi.org/10.1093/abt/tbaf006
Research Article

# Preclinical development of mecbotamab vedotin (BA3011), a novel, AXL-specific conditional active biologic antibody–drug conjugate

Hwai Wen Chang*, Jing Wang, Haizhen Liu, Charles Xing, Jian Chen, Gerhard Frey, William J. Boyle, Jay M. Short*

Research & Development, BioAtla Inc., San Diego, CA 92121, United States

*Corresponding authors. Hwai Wen Chang, Research & Development, BioAtla Inc., 11085 Torreyana Road, San Diego, CA 92121, United States. E-mail: cchang@bioatla.com; Jay M. Short, Research & Development, BioAtla Inc., 11085 Torreyana Road, San Diego, CA 92121, United States. E-mail: jshort@bioatla.com

## Abstract

**Background:** AXL, a tyrosine kinase receptor, is over-expressed in many solid and hematologic cancers, promoting progression and poor clinical outcomes. It also contributes to resistance against chemotherapeutic agents, especially tyrosine kinase inhibitors, by upregulating AXL signaling or switching oncogenic pathways. These factors make AXL an attractive therapeutic target. However, early attempts with naked antibody therapies failed due to the high doses need for efficacy, and antibody-drug conjugates (ADCs) targeting AXL were hindered by off-tumor toxicities due to its expression on normal tissues.
**Methods:** To address these issues, we developed a novel, conditionally active biologic ADC, mecbotamab vedotin (BA3011), which selectively binds to AXL in the acidic tumor microenvironment. In healthy tissue, binding to AXL is substantially diminished due to a powerful selection mechanism utilizing naturally occurring, physiological chemicals referred to as Protein-associated Chemical Switches. BA3011 was tested in vitro and in vivo against AXL expressing cancer cells.
**Results:** Mecbotamab vedotin demonstrates the expected AXL, tumor-specific binding properties and effectively induced lysis of AXL-positive cancer cell lines in vitro. In vivo, mecbotamab vedotin exhibited potent and lasting antitumor effects in human cancer xenograft mouse models. Furthermore, in nonhuman primates, mecbotamab vedotin demonstrated excellent tolerability at doses of up to 5 mg/kg and maintained linker-payload stability in vivo.
**Conclusions:** These findings indicate that mecbotamab vedotin has the potential to be a robust and less toxic therapeutic agent, offering promise as a treatment for patients with AXL-positive cancers.

**Statement of Significance**
A tumor-targeting anti-AXL antibody–drug conjugate with a novel pH-dependent binding mechanism was generated and preclinically characterized *in vitro* and *in vivo*. The conditional, tumor-selective target binding properties reduce on-target, off-tumor toxicities and widen the therapeutic index allowing clinical testing in important cancer indications.

**Keywords:** AXL; mecbotamab; antibody–drug conjugate; conditional active biologic; tumor microenvironment

## Introduction

AXL is a 140-kDa protein of the TAM family of receptor tyrosine kinases, which includes TYRO3, AXL, and MER. AXL is composed of two N-terminal immunoglobulin (Ig)-like domains, two type 3 fibronectin repeats in the extracellular domain, a transmembrane region, and a tyrosine kinase domain in the cytoplasmic domain. Growth Arrest Specific-6 (GAS6), a vitamin K-dependent protein, binds to AXL with higher affinity compared to TYRO3 and MER. Binding of GAS6 to AXL results in AXL homo-dimerization. This activates downstream signaling pathways that regulate cell growth and migration in normal tissues. In tumors it controls drug resistance, immune evasion, epithelial-to-mesenchymal transition (EMT), and metastasis [1, 2]. AXL also heterodimerizes with other TAM family members, as well as with non-TAM family kinases. Furthermore, AXL is known to engage in functional crosstalk with other kinase signaling pathways, increasing its functional complexity [3, 4]. AXL is expressed in a wide variety of normal tissues and the effects of AXL activation are cell- and tissue-specific. AXL assists in maintaining normal hematopoiesis and plays an important role in erythroid differentiation and platelet function. Additionally, AXL is involved in leukocyte differentiation and function, particularly for natural killer (NK) and myeloid cells. Macrophage and monocytes are critically dependent on AXL function for mediating clearance of apoptotic cells and regulation of the innate immune response by limiting inflammation. Vascular smooth muscle cells have high AXL

**Received:** August 21, 2024. **Revised:** February 2, 2025. **Accepted:** February 28, 2025
© The Author(s) 2025. Published by Oxford University Press on behalf of Antibody Therapeutics. All rights reserved. For permissions, please e-mail: journals.permissions@oup.com.

Downloaded from https://academic.oup.com/abt/advance-article/doi/10.1093/abt/tbaf006/8110027 by guest on 17 April 2025

expression, which aids in protection during vascular injury by increasing cell viability, reducing apoptosis, and aiding in tissue remodeling [3, 5].

Given AXL's multiple roles in cell maintenance, it is perhaps not surprising that AXL overexpression on tumor cells is a feature of many cancer types [3, 4, 6]. In this setting, AXL signaling contributes to cell proliferation, resistance to apoptosis, and invasion by mediating EMT. AXL is also implicated in mechanisms of resistance to chemotherapeutics, particularly tyrosine kinase inhibitors, through either direct upregulation of AXL signaling or by switching of oncogenic signaling pathways to maintain high proliferation rates [7, 8]. AXL signaling has recently been implicated as a mechanism involved in the adaptive resistance to mutant KRAS (G12C) inhibition by adagrasib and sotorasib [9]. Recently, functionally activating AXL mutations have been identified in myxofibrosarcoma [10]. In addition, AXL is expressed on tumor-associated macrophages, and its signaling function is involved in the intratumoral transition of M2 tumor suppressive myeloid cells [11]. The diverse role of AXL in facilitating cancer progression and its presence on immunosuppressive cell types in the tumor microenvironment (TME), make it an attractive therapeutic target [1, 12, 13].

AXL-targeting therapeutic agents with different modes of action have been developed, including small molecule kinase inhibitors, monoclonal antibodies (mAbs), and soluble receptors designed to block AXL activation or the downstream signaling pathway (reviewed in Bhalla *et al.* [14]), as well as antibody–drug conjugates (ADCs) that directly eliminate the cancer cells through their cytotoxic payloads.

Bemcentinib (BGB324), an AXL-selective kinase inhibitor, along with INCB081776 and ONO-7475 (both specific for AXL and MERTK), as well as a few other kinase inhibitors, are in clinical development for the treatment of hematological cancers and solid tumors, either as monotherapy or in combination with other kinase inhibitors or immune checkpoint inhibitors [14]. However, several toxicities have been reported in ongoing clinical trials of bemcentinib, including elevations in liver transaminases [15], hematological toxicit,y, and diarrhea [14, 16]. In addition, inhibiting TAM receptors and their ligands can impair the removal of apoptotic cells by macrophages and dendritic cells. The accumulation of apoptotic cells can lead to autoimmune responses, as well as ocular and central nervous system (CNS) toxicity [17]. ADCs are a rapidly growing class of antitumor therapeutics that deliver highly potent cytotoxic agents via mAbs targeting tumor-associated antigens (TAAs) [17]. The overarching principle of ADCs is relatively straightforward: (i) the mAb portion of the ADC selectively binds to the antigen on the tumor cell surface, allowing the receptor–ADC complex to be internalized through the endocytosis pathway and transported to intracellular organelles and (ii) the linker is subsequently cleaved by endogenous enzymes, releasing the cytotoxic drug from the antibody and enabling the payload to induce cytotoxic effects through various mechanisms of action such as binding to DNA or tubulin to inhibit cell replication [18]. In practice with traditional ADCs, factors such as the relative distribution of target antigen on normal tissue, the degree of ADC internalization by target cells, overall stability of the linker-payload in blood and clearance of free, circulating cytotoxic agent meaningfully impact the observed therapeutic index for each ADC.

Three AXL-targeting ADCs have entered early clinical development so far: Enapotamab Vedotin (clinical development discontinued), Mecbotamab Vedotin (preclinical development described in this report), and Mipasetamab Uzoptirine (clinical development discontinued) [19, 20],

Mecbotamab was developed using BioAtla's conditionally active biologic (CAB) technology. This is a novel antibody generation platform that leverages the differential binding of naturally occurring Protein-associated Chemical Switches™ (PaCS™) on target molecules, yielding antibodies that have no or very little binding to the target antigens in healthy tissue (normal alkaline physiological conditions; pH $\geq$ 7.4), but have strong binding in the context of cancer cells (TME: pH 5.3 to 6.7) [21–23]. Using CAB technology, we have developed a novel anti-AXL CAB-ADC, mecbotamab vedotin (BA3011), which allows the preferential targeting of tumor tissues thereby increasing the efficacy to toxicity ratios (therapeutic index). Here, we describe the results of several *in vitro* and *in vivo* pharmacology studies, which collectively show that BA3011 selectively binds to human and cynomolgus monkey AXL in acidic conditions reflective of the TME but has reduced binding under normal alkaline tissue conditions. BA3011 induced the cytotoxicity of human tumor cell lines expressing AXL *in vitro* and inhibited tumor growth in human tumor xenografts *in vivo*. Finally, BA3011 was well tolerated in nonhuman primate (NHP) toxicity studies. These findings indicate that BA3011 is a promising approach to the treatment of AXL expressing cancers. Furthermore, BA3011 (mecbotamab vedotin) has shown encouraging early results in patients with advanced malignancies, including non-small cell lung carcinoma [24], sarcoma [25], and adenoid cystic carcinoma [26].

## Materials and methods

### Generation of AXL-specific conditionally active antibodies and drug conjugates

Antibodies against human AXL were developed by immunizing BALB/c mice (Genscript) with recombinant human AXL extracellular domain (huAXL-ECD-His; Sinobiological, catalog no. 10279-H08H). Hybridomas were generated from mice with AXL-specific serum antibodies (tested by ELISA with recombinant huAXL ECD-His and by FACS using Chinese hamster ovary [CHO] cells expressing human AXL on the cell surface). Hybridoma clones producing AXL-specific mAbs were identified as described above and mRNA was extracted and sequenced.

Variable domains from hybridomas binding to recombinant human and cynomolgus AXL extracellular domains as well as human and cynomolgus AXL expressed on the cell surface were cloned, expressed as human IgG1/kappa chimeras, and further characterized for their binding and *in vitro* functional activities. Selected clones were conjugated with monomethyl auristatin E (MMAE) and tested for cell-killing activity *in vitro*.

Chimeric clone BA-063-10F10 was humanized using BioAtla's proprietary Express Humanization™ protocol and one of the humanized variants, clone BA-063-hum10F10, was selected for further engineering and the development of a CAB antibody [22].

A library of variants of clone BA-063-hum10F10 with mutations introduced in all six CDR loops was screened for binding to recombinant human AXL-ECD at pH 6.0 (TME condition) and pH 7.4 (normal alkaline physiological condition). Screening yielded several clones with the desired properties (high binding at pH 6.0; low binding at pH 7.4). Acidic extracellular pH is a key characteristic of the TME because of the glycolytic metabolism of cancer cells that underpins the continuous replication of cancer cells [27].

Lead CAB clone BA301 and isotype control clone B12 (specific for GP120) were conjugated with MMAE containing a valine-citrulline protease cleavable dipeptide as previously described

Downloaded from https://academic.oup.com/abt/advance-article/doi/10.1093/abt/tbaf006/8110027 by guest on 17 April 2025

[28]. BA3011, the resulting ADC from clone BA301 (drug to antibody ratio 4:1, DAR4, Supplementary Fig. S1B), was characterized *in vitro* and *in vivo* and is described further in this report. This lead CAB antibody BA301 and a pH 7.4 affinity-matched parent antibody were conjugated to the highly potent DNA-targeting cytotoxin PNU (DAR4), an anthracycline derivative related to the established cancer drug doxorubicin (see Supplemental figures and methods).

## Cell lines and cell culture

LCLC-103H, a human large cell lung carcinoma cell line (DSMZ, catalog no. ACC384), was cultured in RPMI 1640 media (Gibco, catalog no. 11875-085) supplemented with 10% fetal bovine serum (FBS) (Gibco, catalog no. 16140-071). DU145, a human prostate carcinoma cell line (ATCC, catalog no. HTB-81), was cultured in minimal essential medium (MEM) (Gibco, catalog no. 11095-072) supplemented with 10% FBS, 1× nonessential amino acids (NEAA) (Sigma, catalog no. M7145) and 1× sodium pyruvate (Corning, catalog no. 25-000-CI).

293-F cell was derived from the HEK293 cell line, a primary embryonal human kidney cell line transformed with sheared human adenovirus type 5 DNA (ThermoFisher, catalog no. R79007) and cultured in MEM (Gibco, catalog no. 11095-072) supplemented with 10% FBS. 293-F cells expressing human AXL ECD (293 huAXL), cynomolgus monkey AXL ECD (293 cynoAXL), or human MER tyrosine kinase (huMERTK) ECD on the cell surface were created at BioAtla and cultured in MEM supplemented with 10% FBS and 1 mg/ml of G418 (Invivogen, catalog no. ant-gn-5). CHO-S cells expressing human TYRO3 ECD on the cell surface were created at BioAtla and cultured in DMEM (Gibco, catalog no. 11965-084) supplemented with 10% FBS and 1 mg/ml of G418 (Invivogen, catalog no. ant-gn-5). All cells were maintained at 37°C and 5% $CO_2$ in a humidified atmosphere and routinely subcultured twice per week. The cells were harvested when in the exponential growth phase for use in the experiments described in the following.

## Epitope mapping

The human and mouse AXL tyrosine kinase extracellular domains consist of two Ig-like and two fibronectin type 3-like domains. BA301 does not cross-react with mouse AXL. To determine the binding region of BA301 on human AXL, four human/mouse chimeric AXL extracellular domains were created. In each chimeric molecule, one of the Ig-like domains or one of the fibronectin type 3-like domains was exchanged with the corresponding mouse sequence.

The four chimeric genes (hAXL-mIg-1, hAXL-mIg-2, hAXL-mFN3-1, and hAXL-mFN3-2) were synthesized with a C-terminal His-tag, expressed in HEK293 cells, and purified using a His-Trap HP column (Cytiva, catalog no. 17524801). Binding of BA301 to each of the four chimeric AXL molecules was tested by affinity enzyme-linked immunosorbent assay (ELISA) (pH 6.0) as described in the following. Human AXL extracellular domain (Sinobiological, catalog no. 10279-H08H) was used as positive control.

## pH affinity ELISA

Human recombinant AXL antigen (Sinobiological, catalog no. 10279-H08H) was immobilized in the wells of a 96-well ELISA plate at 1 $\mu$g/ml in carbonate bicarbonate coating buffer (Sigma, catalog no. C3041-100CAP) overnight at 4°C. Plates were blocked with either pH 6.0 ELISA assay incubation buffer [phosphate-buffered saline (PBS) with 2.5 g/l sodium bicarbonate, 2% nonfat milk, pH 6.0] or pH 7.4 ELISA assay incubation buffer (PBS with 2.5 g/l sodium bicarbonate, 2% nonfat milk, pH 7.4) at room temperature for 1 hour then washed with the corresponding pH ELISA wash solution (PBS with 2.5 g/l sodium bicarbonate, 0.05% Tween-20). BA3011 ADC was serially diluted in the corresponding pH ELISA assay incubation buffer and added to the previously blocked and washed wells. ELISA plates containing the diluted antibodies were sealed and incubated at room temperature for 1 hour while shaking. The plates were washed three times with the corresponding pH ELISA wash buffer, then 100 $\mu$l of antihuman IgG antibody horseradish peroxidase (HRP) secondary antibody (Promega, catalog no. W4031) diluted 1:2500 in the corresponding pH ELISA assay incubation buffer was added to each well. Subsequently, the plates were sealed and incubated at room temperature for 1 hour while shaking. Following incubation, the plates were washed three times with the corresponding pH ELISA wash buffer. About 100 $\mu$l of 3,3,5,5-tetramethylbenzidine (TMB) peroxidase substrate solution (Promega, catalog no. G743X) was added to each well and the reactions were stopped after 3 minutes with 100 $\mu$l of 0.1 N HCl (Beijing Reagent, catalog no. G81788B). The optical density (OD) at 450 nm was collected using a Microplate Spectrophotometer (ThermoFisher, Multiskan™ SkyHigh). The half-maximal effective concentration ($EC_{50}$) values for binding to human AXL ECD at pH 6.0 and pH 7.4 were determined using the nonlinear fit model (variable slope, four parameters) of GraphPad Prism version 7.03.

## pH range ELISA

The activity of BA3011 was tested in a range of pH ELISA assay conditions (pH 6.0 to pH 7.4) mimicking the TME (pH 6.0 to pH 6.7) and normal alkaline physiological conditions (pH ≥ 7.4). Human recombinant AXL antigen (Sinobiological, catalog no. 10279-H08H) was immobilized in the wells of a 96-well ELISA plate at 1 $\mu$g/ml in carbonate bicarbonate coating buffer (Sigma, catalog no. C3041-100CAP) overnight at 4°C. Plates were blocked with various pH ELISA assay incubation buffers (PBS with 2.5 g/l sodium bicarbonate, 2% nonfat milk at pH 6.0, 6.2, 6.5, 6.7, 7.0, and 7.4) at room temperature for 1 hour then washed with the corresponding pH ELISA wash buffer (PBS with 2.5 g/l sodium bicarbonate, 0.05% Tween-20). About 30 ng/ml of BA3011 antibody was diluted in the corresponding pH ELSA assay incubation buffer and added to the wells which were previously washed and blocked. The ELISA plates were sealed and incubated at room temperature for 1 hour with shaking, then washed with the corresponding pH ELISA wash buffer three times. The ELISA plates were then read as described in the pH affinity ELISA procedure by antihuman IgG HRP secondary antibody. The amount of test sample bound to human AXL under the different pH assay conditions was measured by absorbance at 450 nm using a Microplate Spectrophotometer. The pH inflection points that demonstrated 50% binding activity at varying pHs compared to pH 6.0 (set as 100%) were determined using the nonlinear fit model (variable slope, four parameters) of GraphPad Prism version 7.03.

## Cross-species ELISA

Human recombinant AXL antigen (Sinobiological, catalog no. 10279-H08H), cynomolgus monkey recombinant AXL antigen (BioAtla), mouse recombinant AXL antigen (Sinobiological, catalog no. 50126-M08H), and rat recombinant AXL antigen (BioAtla) were immobilized in the wells of a 96-well ELISA plate at 1 $\mu$g/ml in carbonate bicarbonate coating buffer (Sigma, catalog no. C3041-100CAP) overnight at 4°C. The cross-species ELISA was performed following the same method as described for the pH affinity ELISA and the data were analyzed using the nonlinear fit model (variable slope, four parameters) of GraphPad Prism version 7.03.

Downloaded from https://academic.oup.com/abt/advance-article/doi/10.1093/abt/tbaf006/8110027 by guest on 17 April 2025

## pH flow cytometry

The binding affinity of BA3011 to human and cynomolgus monkey-AXL expressing HEK293 stable cells, as well as human AXL-expressing tumor cell lines was measured by flow cytometry under pH 6.0 and pH 7.4 conditions. B12 (anti-GP120 antibody [29] produced by evitria AG (Zűrich, Switzerland) conjugated with MMAE at a similar DAR was used as the isotype control. Briefly, the cells in log phase were detached and seeded in 96-well round bottom plates on the day of assay. Cells were washed once with pH flow cytometry assay buffer [PBS with 2.5 g/l sodium bicarbonate and 1% bovine serum albumin (BSA)] of pH 6.0 or pH 7.4 and pelleted by centrifuge. Antibodies that had been serially diluted in pH flow cytometry assay buffer were added to the cells and incubated for 1 hour at 4°C in the dark with shaking. The mixture containing cells and antibodies was spun down and washed with the corresponding pH flow cytometry assay buffer three times. The secondary antibody (goat antihuman IgG, Invitrogen, catalog no. A11013) conjugated with fluorophore Alexa 488 was then added to each well and incubated for 45 min at 4°C in the dark with shaking. Cells were then washed with pH assay buffer three times, and fixed with 4% paraformaldehyde (Electron microscopy sciences, catalog no. 15710). The median fluorescence intensity (MFI) was then collected with a NovoCyte flow cytometer (ACEA Biosciences, model 2060R). MFI and antibody concentrations were used to generate four-parameter nonlinear regression curves with variable slope using GraphPad Prism software version 9.0. $EC_{50}$ values for antibody binding to the target cells were calculated at pH 6.0 and pH 7.4.

## Internalization analysis of BA3011

293-huAXL cells were incubated with BA3011 in ice-cold assay buffers at pH 6.0 or pH 7.4 (60 min). FITC conjugated antihuman IgG antibody (Thermo Scientific, catalog no. 31513) was added and after additional incubation on ice (60 minutes) the cells were transferred to pH culture medium (DMEM + 10% FBS, pH 6.0 or pH 7.4) and incubated at 37°C for the indicated time periods. At each time point, two aliquots of cell sample were collected. One aliquot was directly fixed by 4% PFA and the FITC fluorescence was detected as the total FITC signal. The other aliquot was stained with Biotin-conjugated anti-FITC monoclonal antibody (eBioscience, catalog no. 13-7691-82) in pH assay buffers to quench the surface FITC signal, and the FITC fluorescence was collected as the cytoplasmic signal. The surface signal was calculated by the total signal subtracted by the corresponding cytoplasmic signal.

## Kinetic analysis of pH-dependent binding of BA3011

Binding kinetics of BA3011 to AXL were analyzed by surface plasmon resonance (SPR) on a SPR 2/4 instrument (Sierra Sensors, Hamburg, Germany). In brief, varying antibody concentrations were injected over a sensor surface with immobilized human or cynomolgus monkey AXL. Binding kinetics were analyzed with a 1:1 binding model with the provided analysis software (Sierra Analyzer R2, Bruker). A molecular weight of 150 kDa was used to calculate the molar concentrations of the BA3011 analyte.

## *In vitro* cytotoxicity

The cytotoxicity of BA3011 or isotype control (B12-MMAE) was tested in the LCLC-103H large cell lung carcinoma cell line, DU145 prostate cancer cell line and 293-F cells (AXL negative cell line). Cells were seeded in 50 $\mu$l of pH assay medium (DMEM + 1× NEAA + 1× sodium pyruvate+10% FBS, adjusted to pH 6.0 or pH 7.4) at 2000 cells per well in 96-well tissue culture-treated plates and incubated overnight in a humidified incubator at 37°C containing 5% $CO_2$. Serial dilutions of 2× BA3011 stock solution in pH 6.0 or pH 7.4 assay media (50 $\mu$l per well) were added to the plates. After a 3-day incubation, the cell viability was measured with the CellTiter-Glo (Promega Corporation) reagent, and the luminescence was recorded on the SpectraMax i3X plate reader. The inhibition rate (IR) of BA3011 or isotype control antibody was determined by the following formula: IR (%) = [1 − (RLU compound/RLU control)] × 100%. The IRs of different antibody concentrations were plotted in concentration–response inhibition curves and the half-maximal inhibitory concentration ($IC_{50}$) was calculated. The data were interpreted by GraphPad Prism software using a four-parameter logistic nonlinear regression model. A total of three independent cell-based killing experiments were performed for each of the two cell lines tested.

## *In vivo* efficacy studies

The antitumor activity of BA3011 was assessed using different cell line-derived xenograft (CDX) models, including the LCLC-103H large cell lung carcinoma cell line (performed at Crown Bioscience), the DU145 prostate cancer cell line (performed at Crown Bioscience), and the MIA PaCa-2 pancreatic cancer cell line (performed at WuXi AppTec).

For the LCLC-103H CDX model, female NOD/SCID mice were implanted with $10 \times 10^6$ tumor cells subcutaneously into the rear flank. When tumor volume reached 100–150 $mm^3$, animals were randomized into groups of eight animals and injected intravenously (IV) with vehicle or BA3011 at three dose levels (1, 3, or 6 mg/kg) once every 4 days for a total of six injections (Q4DX6).

For the MiaPaCa-2 CDX model, female NOD/SCID mice were implanted with $10 \times 10^6$ tumor cells subcutaneously into the rear flank. When tumor volume reached 100–150 $mm^3$, animals were randomized into groups of eight animals and injected IV with vehicle or BA3011 at four dose levels (1, 3, 6, or 10 mg/kg) once every 4 days for a total of four injections (Q4DX4).

For the DU145 CDX model, male BALB/c nude mice were implanted with $5 \times 10^6$ tumor cells subcutaneously into the rear flank. When tumor volume reached 150–250 $mm^3$, animals were randomized into groups of eight animals and injected IV with vehicle or BA3011 at three dose levels (6, 10, or 15 mg/kg), once every 4 days for total of six injections (Q4DX6).

In each CDX model above, tumor size and animal body weight were monitored regularly. Antitumor activity was measured by % tumor growth inhibition (TGI), which indicates the tumor volume change between vehicle-treated control group and the test article-treated cohort.

## *In vivo* pharmacokinetics and toxicology in nonhuman primates

A non-Good Laboratory Practice (GLP) dose-range finding (DRF) study and a GLP compliant repeat-dose toxicity study were performed to evaluate the pharmacokinetics (PK) and toxicity of BA3011 in cynomolgus monkeys (LabCorp). In the DRF study, male and female cynomolgus monkeys (one animal/sex/group) were administered BA3011 at 1, 3, and 10 mg/kg by IV bolus. Animals were observed for 21 days. Safety endpoints included clinical observations, food consumption, body weight, hematology, coagulation, serum chemistry, and urinalysis. Blood was collected at multiple time points to characterize systemic exposure of BA3011. Immunophenotyping of peripheral blood was conducted by flow cytometry. At termination, gross observations and organ weights

Downloaded from https://academic.oup.com/abt/advance-article/doi/10.1093/abt/tbaf006/8110027 by guest on 17 April 2025

were recorded, and tissues were collected for microscopic evaluation.

In the repeat-dose toxicity study, two doses of BA3011 were administered by IV bolus 3-weeks apart (day 1 and day 22) to male and female cynomolgus monkeys (five animals/sex/group) at 0 (vehicle control), 1, 5, and 10 mg/kg/week. On day 23 a necropsy was performed on surviving animals (three animals/sex/group) while the remaining animals were placed into a 4-week recovery period to assess reversibility of any toxicological effects. Safety endpoints included clinical signs, body weights, ophthalmic exams, electrocardiograms (ECGs), body temperature, clinical pathology (clinical chemistry, coagulation, hematology, and urinalysis), organ weights, as well as macroscopic and microscopic examinations. Blood samples were collected to evaluate systemic exposure to BA3011 and for potential formation of antidrug antibodies (ADA). In a single dose study in cynomolgus monkeys the PK of BA301-PNU was compared to a non-CAB, affinity-matched parent (AM-NONCAB-PNU) (SNBL, WA, USA).

# Results

## Engineering of anti-AXL conditionally active biologics

This study aimed to generate a novel, CAB ADC with reduced binding to AXL under normal alkaline physiological conditions (pH ≥ 7.4) while maintaining strong binding under acidic TME conditions (pH 5.3–6.7) [21, 27]. AXL-specific hybridomas were sequenced, expressed as chimeric IgG1 antibodies, and screened for cross reactivity with cynomolgus AXL and internalization. Clone BA-063-10F10 was humanized. Humanized clone BA-063-hum10 was then engineered for conditional binding to AXL under TME conditions (Supplementary Fig. S1A). The *in vitro* and *in vivo* characterization of lead molecule BA3011 (mecbotamab vedotin) is described further in this report.

## *In vitro* characterization of BA3011

The binding activity of BA3011 to human AXL-ECD at pH 6.0 (TME conditions) and pH 7.4 (physiological conditions) was tested by pH affinity ELISA (Fig. 1A). BA3011 showed strong binding to human AXL at pH 6.0 with an $EC_{50}$ of 4.78 ng/ml. At pH 7.4, minimal binding was observed at the highest concentrations tested, but no meaningful $EC_{50}$ could be calculated (Fig. 1A). BA3011 binding to human AXL was tested at pH 6.0, 6.2, 6.5, 6.7, 7.0, and 7.4 (pH range ELISA, Fig. 1B). BA3011 showed strong binding to human AXL at pH 6.0 to ∼6.4. At higher pH the binding activity dropped and minimal binding was detectable at pH 7.0–7.4. The pH inflection point (pH with 50% signal compared to pH 6.0 set as 100%) was at pH 6.6. The pH range ELISA data clearly shows reduced binding at physiological pH, which should equate to reduced AXL binding in healthy, normal tissues.

BA3011 bound to cynomolgus AXL at pH 6.0 with a similar binding profile as to human AXL and showed very little binding at pH 7.4 (Fig. 1C). BA3011 did not bind to mouse or rat AXL regardless of the pH (Fig. 1C). In addition, BA3011 is specific for AXL and does not bind to the other two TAM family members, TYRO3 or MER (Fig. 1D).

The AXL extracellular domain consists of two Ig-like and two fibronectin type 3-like domains (Supplementary Fig. S2A). To determine the biding area of BA301, four chimeric human/mouse AXL extracellular domains were generated, where each human domain was replaced with the corresponding mouse domain. Binding of BA301 to each of these chimeric molecules was tested by ELISA at pH 6.0 (Supplementary Fig. S2B, blue bars). BA301 does not bind to the chimeric AXL proteins that contain either mouse Ig-1 or Ig-2 domains. Switching the fibronectin type 3-like domains to the corresponding mouse domains does not affect the binding. This indicates that BA301 contacts residues on both Ig-like domains. The non-CAB parent clone shows the same binding pattern (Supplementary Fig. S2B, red bars), indicating that conditional binding of BA301 does not change the binding region. AXL forms a homodimer with two GAS6 molecules [30]. There are four residues close to the Ig-1/Ig-2 interface that differ in mouse and human AXL (Supplementary Fig. S2C, orange spheres), which could be the potential contact points for BA301.

The binding activity of BA3011 to various human AXL expressing cell lines as well as 293-F cells expressing cynoAXL in TME pH (pH 6.0) and normal physiological conditions (pH 7.4) was also measured by flow cytometry (Fig. 2A and B). At pH 6.0, BA3011 bound to cell-surface expressed human AXL with an $EC_{50}$ between 16 ng/ml (DU145 cells) and 37.0 ng/ml (LCLC-103H cells). BA3011 bound to cell-surface expressed cynomolgus AXL (293-cynoAXL) at pH 6.0 with a similar binding profile as to human AXL and showed very little binding at pH 7.4. As expected, minimal binding of BA3011 was observed at pH 7.4. BA3011 did not bind to naïve 293-F cells, which do not express AXL on the surface. There was no detectable binding of isotype antibody (B12-MMAE) in any of the cell lines tested. AXL expression level of the different cell lines was determined by PE staining (Supplementary Fig. S3).

The binding kinetics of BA3011 were determined by SPR at pH 6.0, pH 6.5, and pH 7.4 using the same sensor chip for all experiments. Representative sensorgrams for each pH condition are shown in Fig. 3A. BA3011 showed a high affinity (sub-nanomolar affinity) to human AXL at the different pH values tested (Fig. 3B). The affinity dropped by ∼3.5-fold from pH 6.0 to pH 7.4 ($K_D$ = 62 to 218 pM, respectively). In addition, the observed SPR signal showed a strong reduction at pH 7.4 compared to pH 6.0 and pH 6.5. The maximum signal at pH 7.4 reaches only 10%–15% of the signal at pH 6.0. This drop in signal intensity at higher pH is characteristic of CABs. We have previously shown that this signal drop is caused by a change in the reversible availability of the reactive ligands on the sensor surface [22]. The number of available reactive ligands drops with an increase in pH. The availability of reactive ligands at different pH conditions is affected by the interaction of the proteins with the charged PaCS molecules, e.g. bicarbonate ions, which block the binding of BA3011 in a concentration-dependent manner. Therefore, the pH selectivity is a combination or product of the change in $K_D$ and the fold change in the maximum signal observed, leading to substantial selectivity for binding to targets on cancer cells versus those on normal cells.

## *In vitro* cytotoxicity

The ability of BA3011 to inhibit cell viability was assessed in the LCLC-103H human large cell lung carcinoma and DU145 human prostate cancer cell lines, both of which endogenously express AXL. After overnight incubation, the seeded cells were treated with increasing concentrations of BA3011 and an isotype control ADC (B12-MMAE) at either pH 6.0 or pH 7.4, and cell viability was measured after 3 days.

As shown in Fig. 4, BA3011 induced dose-dependent inhibition of cell viability both in LCLC-103H (Fig. 4A) and in DU145 (Fig. 4B) cells. At pH 6.0, BA3011 $IC_{50}$ values were 474 ± 171 and 1466 ± 348 ng/ml for LCLC-103H and DU145, respectively. Higher $IC_{50}$ values were observed in pH 7.4 assay media (1095 ± 231 and 5069 ± 185 ng/ml for LCLC-103H and DU145, respectively). These data are summarized in Fig. 4D. Limited activity of the isotype ADC was observed, although the highest concentration

Downloaded from https://academic.oup.com/abt/advance-article/doi/10.1093/abt/tbaf006/8110027 by guest on 17 April 2025

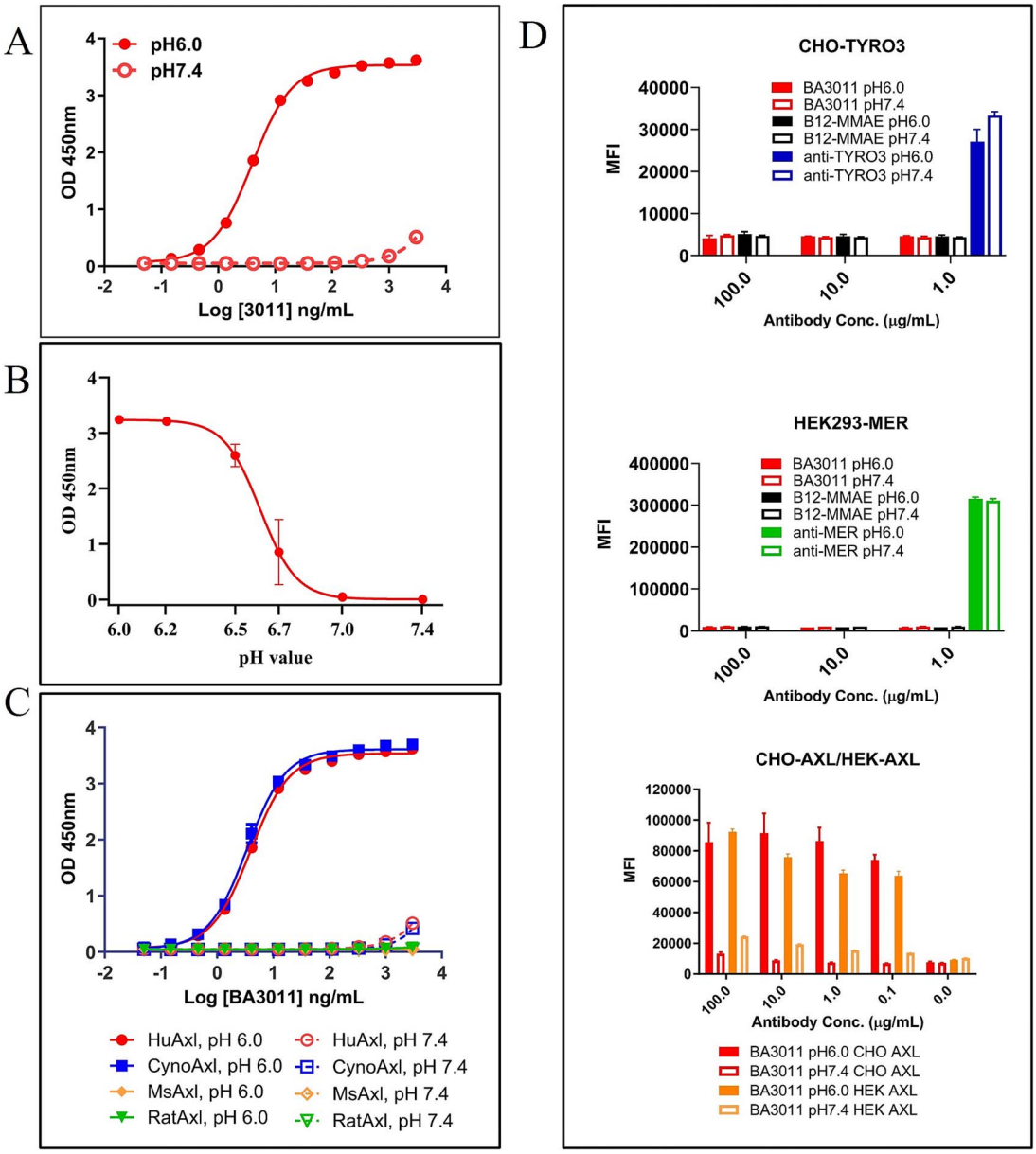


Figure 1. *In vitro* characterization of BA3011. (A) pH affinity ELISA. Binding of BA3011 to human AXL at pH 6.0 (filled circles) and pH 7.4 (open circles) was determined by ELISA with a series of antibody concentrations as indicated. (B) pH range ELISA. Binding of BA3011 to human AXL at different pH values as indicated in the graph was determined by ELISA. The pH inflection point (50% binding activity compared to pH 6.0) was at pH 6.6. (C) Cross species ELISA. Binding of BA3011 to human (circles), cynomolgus (squares), mouse (diamonds), and rat (triangles) AXL at pH 6.0 (filled symbols) and pH 7.4 (open symbols) was determined by ELISA. (D) Specificity evaluation. Binding specificity of BA3011 at pH6.0 (filled bars) and pH7.4 (open bars) to AXL (bottom panel) was tested by flow cytometry using CHO cells transfected with human TYRO3 (top panel) or to HEK293 cells transfected with human MER (middle panel) To confirm TYRO3 and MER expression, cells were stained with TYRO3- or MER-specific antibodies. B12-MMAE was used as isotype control.

resulted in detectable cell growth inhibition. No significant cell cytotoxicity was found in the AXL-negative cell line 293-F (Fig. 4C). These findings collectively demonstrated that BA3011 mediates cytotoxicity in an antigen- and concentration-dependent manner and achieves greater cell killing potency in acidic TME conditions.

Furthermore, the internalization assay of BA3011 into target-expressing 293-huAXL cells demonstrated that different pH conditions did not impact the intracellular trafficking profile of BA3011 (Supplementary Fig. S4). This indicates that the enhanced killing potency of BA3011 at pH 6.0 is primarily due to its increased affinity for the AXL target in acid conditions.

## BA3011 inhibits tumor growth *in vivo*—human cancer cell line xenograft

The *in vivo* activity of BA3011 was evaluated in several CDX murine models representing three different cancer indications (NSCLC, pancreatic, and prostate cancer). In the LCLC-103H xenograft model, NOD/SCID mice were inoculated with LCLC-103H cells and then randomized into groups for dosing with the Q4DX6 regimen. BA3011 exhibited potent antitumor activities at all three dose levels (1, 3, and 6 mg/kg), with TGI of 114%, 113%, and 115%, respectively at day 19 (Fig. 5A). In addition, the 3 mg/kg and 6 mg/kg groups showed sustained antitumor activity for up to 57 days.

Downloaded from https://academic.oup.com/abt/advance-article/doi/10.1093/abt/tbaf006/8110027 by guest on 17 April 2025

A

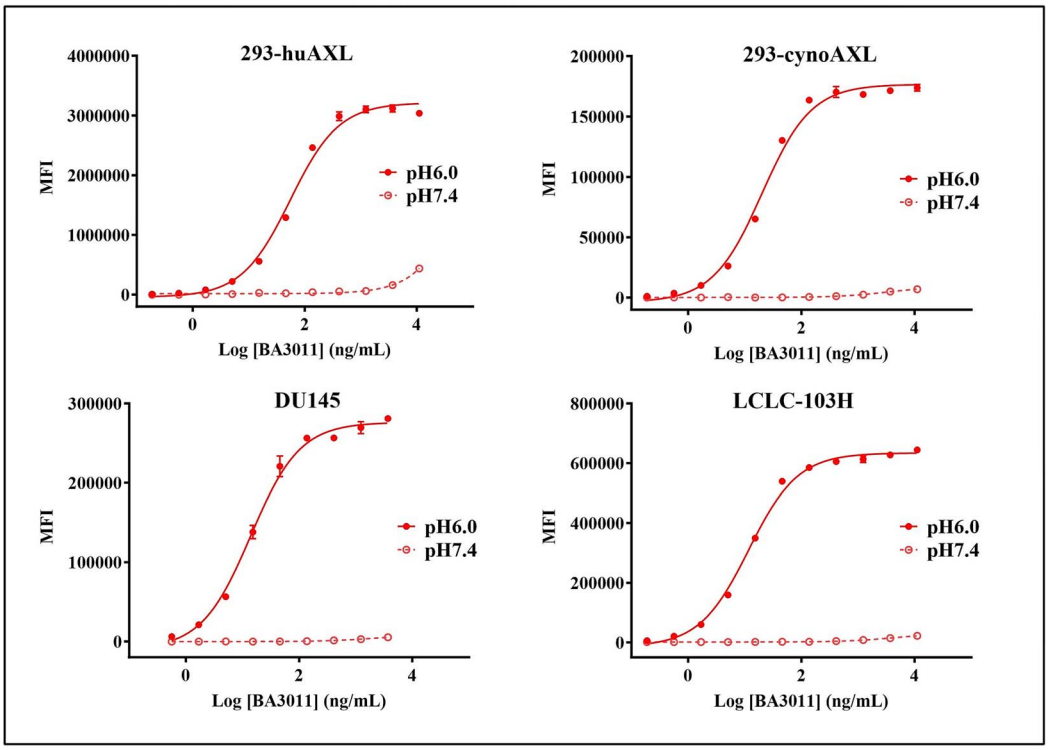


B

| Cell Line | $EC_{50}$ at pH6.0 (ng/mL) |
|---|---|
| 293-hAXL | 56 |
| 293-cynoAXL | 20 |
| DU145 | 16 |
| LCLC-103H | 37 |

Figure 2. Binding of BA3011 to cell-surface expressed AXL analyzed by flow cytometry. (A) Concentration-dependent binding of BA3011 to human (top left panel) or cynomolgus AXL (top right panel) expressed on the surface of 293-F cells and cancer cell lines DU145 (bottom left panel) and LCLC103H (bottom right at pH 6.0 (solid line) and pH 7.4 (dashed line). (B) The table shows the $EC_{50}$ values at pH6.0 calculated from the binding curves shown in (A). No meaningful $EC_{50}$ could be calculated at pH 7.4.

A

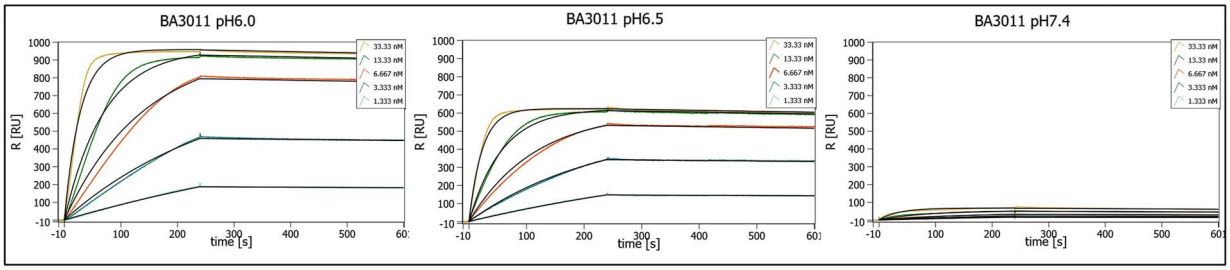


B

| Molecule | BA3011 | | | | | | | | |
|---|---|---|---|---|---|---|---|---|---|
| Method | SPR kinetic measurment | | | | | | | | |
| | pH 6.0 | | | pH 6.5 | | | pH 7.4 | | |
| | $k_a$ [M·s] | $k_d$ [s-1] | $K_D$ [M] | $k_a$ [M·s] | $k_d$ [s-1] | $K_D$ [M] | $k_a$ [M·s] | $k_d$ [s-1] | $K_D$ [M] |
| **Experiment 01** | 1.07E+06 | 6.62E-05 | 6.21E-11 | 1.18E+06 | 9.75E-05 | 8.26E-11 | 5.46E+05 | 1.30E-04 | 2.38E-10 |
| **Experiment 02** | 1.18E+06 | 8.73E-05 | 7.38E-11 | 1.38E+06 | 1.37E-04 | 9.91E-11 | 1.05E+06 | 1.61E-04 | 1.54E-10 |
| **Experiment 03** | 1.09E+06 | 5.49E-05 | 5.05E-11 | 1.31E+06 | 8.45E-05 | 6.46E-11 | 8.60E+05 | 2.25E-04 | 2.62E-10 |
| | | | | | | | | | |
| **Mean** | 1.11E+06 | 6.94E-05 | 6.21E-11 | 1.29E+06 | 1.06E-04 | 8.21E-11 | 8.17E+05 | 1.72E-04 | 2.18E-10 |

Figure 3. BA3011 binding kinetics to human AXL at the indicated pH value measured by SPR. (A) Representative sensorgrams for pH 6.0 (left), pH 6.5 (middle), and pH 7.4 (right). (B) Calculated binding kinetics of BA3011 to human AXL based on 3 independent experiments.

Downloaded from https://academic.oup.com/abt/advance-article/doi/10.1093/abt/tbaf006/8110027 by guest on 17 April 2025

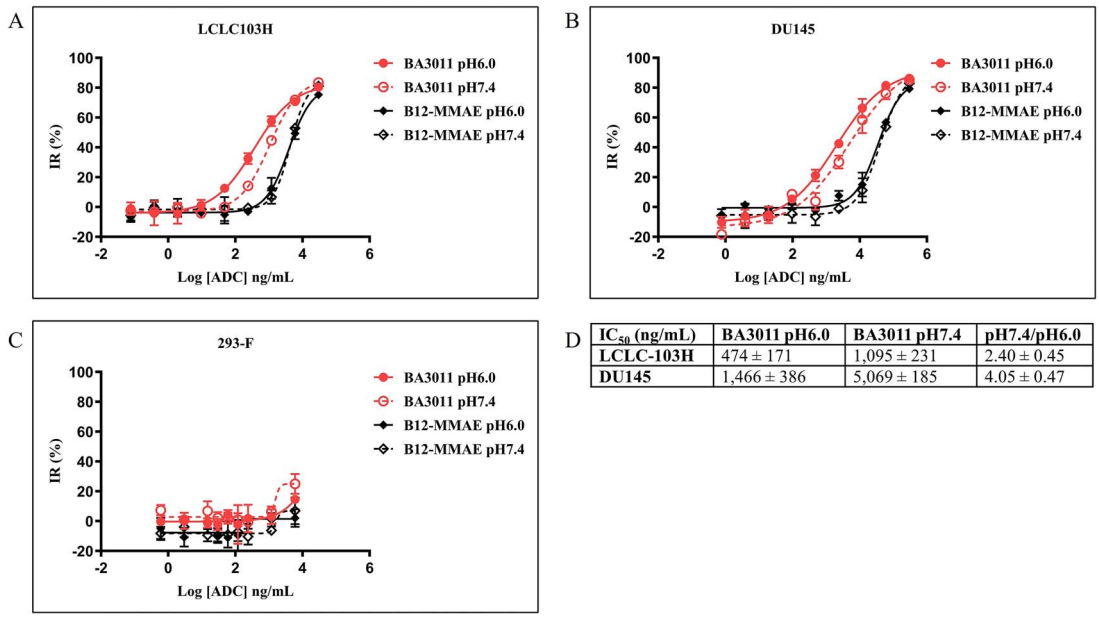


Figure 4. *BA3011 in vitro* cytotoxicity assay. BA3011 *in vitro* cell killing of LCLC103H cells (A), DU145 cells (B), or AXL-negative 293-F cells (C) at pH 6.0 (solid lines) and pH 7.4 (dashed lines). Ctrl: B12-MMAE. (D) $IC_{50}$ values calculated from the inhibition curves from three independent experiments.

In the MIAPaCA-2 human pancreatic cancer cell line xenograft model, BA3011 had strong and dose- dependent antitumor activity. BA3011 at 6 mg/kg significantly inhibited tumor growth by 59% while BA3011 at 10 mg/kg resulted in complete tumor regression (Fig. 5B). In the DU145 human prostate cell line xenograft model, BA3011 also exhibited dose-dependent antitumor activity. BA3011 at 10 mg/kg and 15 mg/kg demonstrated durable antitumor activity, and significantly delayed tumor growth (Fig. 5C). Collectively, results from these *in vivo* xenograft studies suggest that BA3011 treatment could lead to effective and durable antitumor responses.

## Pharmacokinetic, safety and tolerability analysis of BA3011 in nonhuman primates

The nonclinical exposure and safety profile of BA3011 has been characterized by single and repeat dose studies in NHPs up to 1-month in duration, including the assessment of reversibility of test article-related toxicological effects. The PK profile of BA3011 in cynomolgus monkeys was determined after a single IV bolus dose of 1, 3, or 10 mg/kg. The maximum concentration ($C_{max}$), area under the curve from time 0 to the last quantifiable concentration ($AUC_{0\text{-}t}$), and half-life ($t_{1/2}$) are presented in Fig. 6. The AUC of each analyte showed a slightly greater than dose-proportional increase, suggesting the presence of a saturable elimination process for BA3011. Nearly identical results of $C_{max}$, $AUC_{0\text{-}t}$, and $t_{1/2}$ were obtained for total ADC and total antibody (TAb). Plasma concentrations of unconjugated MMAE peaked at 1–2 days post-dose (Fig. 6A).

Bolus IV administration of BA3011 was well tolerated at all doses and there were no unscheduled deaths or observed morbidities. Test article-related changes were confined to transient, decreased white blood cell counts, particularly neutrophils. A similar effect was observed in reticulocyte counts, as well as in $CD3^+$, $CD3^+CD4^+$, $CD3^+CD8^+$, $CD3^-CD20^+$, or $CD3^-CD14^+$ cells and recovered on or before day 21. Exposure for males and females was similar and dose proportional based on $C_{max}$ values and slightly greater than dose-proportional based on $AUC_{0\text{-}t}$. At 10 mg/kg, the mean BA3011 exposure ($AUC_{0\text{-}t}$) was 7120 $\mu$g hour/ml and the $C_{max}$ was 241 $\mu$g/ml, while the $t_{1/2}$ was 46 hrs. The $AUC_{0\text{-}t}$ and $C_{max}$ levels of the released MMAE payload was 0.08 $\mu$g hour/ml and $6.6 \times 10^{-04}$ $\mu$g/ml, respectively (Fig. 6B). In cynomolgus monkeys, the AUC of plasma ADC, TAb, and MMAE increased more than dose proportionally. The BA3011 $t_{1/2}$ showed a dose-proportional increase from 6 hours at 1 mg/kg to 36 hours at 3 mg/kg, and to 46 hours at 10 mg/kg. This indicates a saturable target-mediated disposition of BA3011 has been reported for other ADCs [31]. The primary target organs affected with BA3011 treatment included lymphoid depletion in the thymus, bone marrow, and spleen. These organ changes led to a dose-dependent decrease in white blood cell parameters including significant decreases in neutrophils. The effect on the hematopoietic system was transient and there were no remarkable findings after the 1-month recovery period, consistent with the toxicokinetic profile of other MMAE-containing ADCs and not considered to be due to target engagement in healthy tissues. Interestingly, in a single dose PK study in NHPs comparing BA301 conjugated to PNU and a non-CAB parental version also conjugated to PNU demonstrated that the CAB version had a much longer half-life and exposure than its non-CAB counterpart. This suggests that BA301-PNU did not undergo target mediated drug disposition (TMDD) like the AM-non-CAB PNU ADC and is not interacting with target receptor present on normal tissues (Supplementary Fig. S5).

In the GLP repeat dose toxicity study, administration of BA3011 to cynomolgus monkeys for two doses on days 1 and 22 by slow IV bolus injection at doses of 1, 5, or 10 mg/kg/dose showed no detectable total ADC, TAb, or unconjugated MMAE in samples analyzed from control groups (vehicle control). In general, BA3011 $C_{max}$ was dose-proportional (Fig. 6C and D).

There were no apparent differences in the PK of total and intact antibodies. The peak plasma levels of unconjugated MMAE occurred 24 hours post-dose (Fig. 6C). Unconjugated MMAE circulating $t_{1/2}$ was 41.2–65.5 hours. ADA were detected 3 weeks after the first intravenous dose administration, and generally persisted throughout the treatment and recovery phases (Supplementary Fig. S6). The presence of ADAs did not alter the PK and had no impact on toxicokinetic parameters of BA3011 and

Downloaded from https://academic.oup.com/abt/advance-article/doi/10.1093/abt/tbaf006/8110027 by guest on 17 April 2025

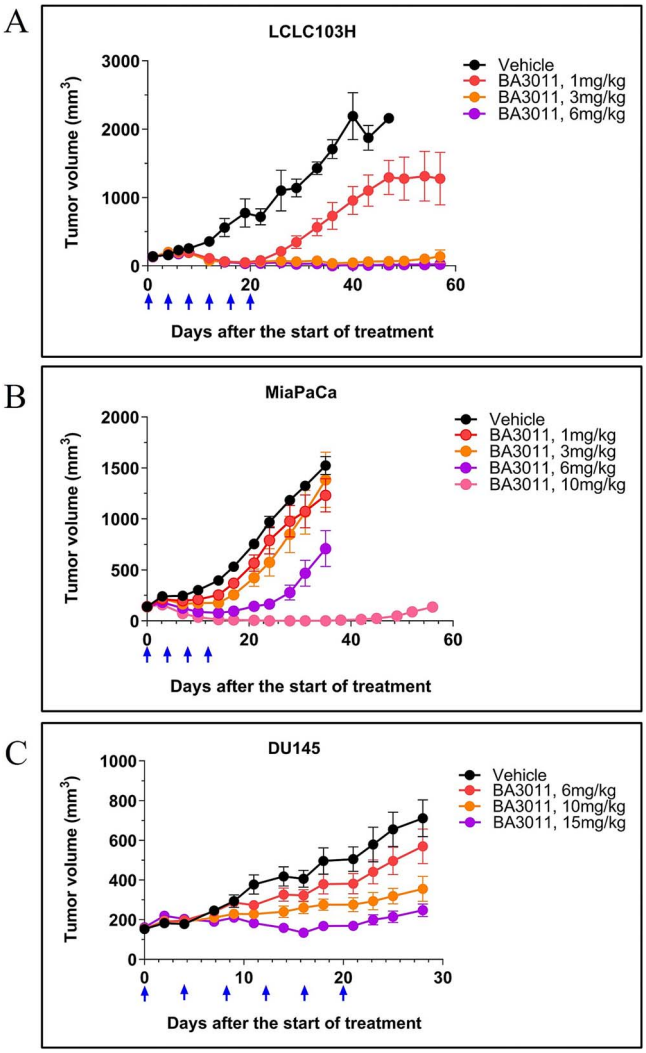


Figure 5. *In vivo* cytotoxicity of BA3011. Cytotoxicity of BA3011 was tested in several cell-line derived tumor models in mice: (A) LCLC103H (lung cancer); (B) MiaPaCa (pancreatic cancer), and (C) DU145 (prostate cancer). Animals were dosed every 4 days (arrows) intravenously with BA3011 or buffer only (vehicle) at the concentrations indicated in the graph.

its components (total ADC, intact antibody, and unconjugated MMAE). ADA formation was not dose-dependent, and did not lead to any immune-mediated toxicities.

Repeat administration of BA3011 showed similar transient effects on neutrophils and lymphocyte levels that recovered after each dose. Adverse hematological changes at 5 and 10 mg/kg/dose in both sexes. Adverse pathological changes in lymphoid organs including minimal to moderate lymphoid depletion in thymus and mild hypocellularity in the bone marrow were observed at 10 mg/kg/dose in males and ≥5 mg/kg/dose in females at the end of the dosing phase; while there were no test article-related microscopic findings in tested organs in any treatment groups with the complete recovery of the thymus and bone marrow at the end of the 4-week recovery phase. These data are also consistent with the effects predicted for MMAE containing ADCs and not considered target related. In the 5 mg/kg/dose and 10 mg/kg/dose group animals, there was no evidence of altered renal function based on evaluation of urinalysis parameters nor were there any microscopic changes within the kidney. Similarly, there were no clinical signs or microscopic changes within the lung or CNS. In addition, there were no BA3011 treatment-related changes in ECG parameters at any dose level, including no evidence of QT prolongation.

## Discussion

Over the past decade, AXL has emerged as a promising therapeutic target in oncology, demonstrating antitumor efficacy by preventing AXL-mediated cancer development, progression, and resistance to therapy [32, 33]. Various therapeutic agents designed to target AXL have been developed, including small molecule inhibitors, mAbs, ADCs, soluble receptors, and chimeric antigen receptor T cells (CAR-T) [8]. Many of these agents have progressed through various stages of clinical development [34], but to date, none have received regulatory approval. Three AXL-targeting ADCs have entered into clinical trials so far. Clinical development for two of them has been stopped. Notably, enapotamab vedotin (payload MMAE, DAR4) was in early clinical development for the treatment of various solid tumors [35]. However, clinical development of this ADC was terminated because of severe (grade 3 or higher) gastrointestinal adverse reactions and low efficacy, which was potentially related to on-target, off-tumor toxicity [36]. The clinical development of Mipasetamab Uzoptirine (payload SG3199 DAR2) was halted during dose optimization/expansion in Phase 1b due to an unfavorable benefit–risk ratio. ADCs represent a promising approach for cancer treatment, as cellular toxins can be more precisely directed to tumor cells through TAAs-specific antibodies. A potent ADC selectively kills tumor cells by binding a TAA via its antibody moiety in a target-dependent manner. Simultaneously, it must induce efficient internalization of the formed antigen–ADC complex to effectively deliver the cytotoxic payload into the tumor cell and release its cytotoxic potential. While AXL is overexpressed in a broad range of tumors [8], its widespread expression in healthy tissues poses a challenge, leading to TMDD and on-target, off-tumor toxicity. Development of our conditionally active AXL-specific ADCs utilizing CAB technology [22], addresses this challenge. CAB AXL antibodies feature optimized binding domains with significantly reduced binding in normal tissue, but high affinity binding in the TME. Importantly, this binding occurs without covalent modification of the antibody or a requirement for enzymatic activity for activation, since our CAB antibodies are not prodrugs. The CAB antibody binding is regulated by extracellular pH and the conditional binding of the PaCS molecules. The CAB antibody has no available targets once it leaves the acidic TME and recirculates into the alkaline microenvironment of normal tissues. Likewise, targets are once again available for binding once it re-enters the acidic TME [22]. The tumor-specific binding does not change the plasma and tissue distribution as this is primarily driven by (passive) diffusion. In contrast to non-CAB AXL-targeting antibodies, the binding of BA3011 to AXL in healthy tissue is highly reduced compared to the tumor.

In this report, we describe the development and characterization of a BA3011 (mecbotamab vedotin) a conditionally active ADC specific for AXL. First, we generated novel AXL-specific antibodies from hybridomas, humanized the lead antibody, and screened a library of variants for conditional binding to AXL in the TME. The CAB generation was performed as previously described [22]. BA3011 was characterized by an *in vitro* binding ELISA and cytolysis assay that replicated the acidic pH conditions of the TME. BA3011 demonstrated tumor-selective binding to human and cynomolgus AXL with a pH inflection point at pH 6.6 (i.e. 50% binding signal compared to pH 6.0) and minimal binding at normal physiological alkaline pH (≥7.4) in an affinity ELISA

Downloaded from https://academic.oup.com/abt/advance-article/doi/10.1093/abt/tbaf006/8110027 by guest on 17 April 2025

A

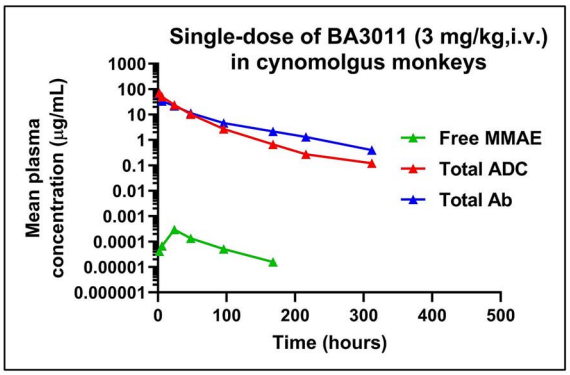


C

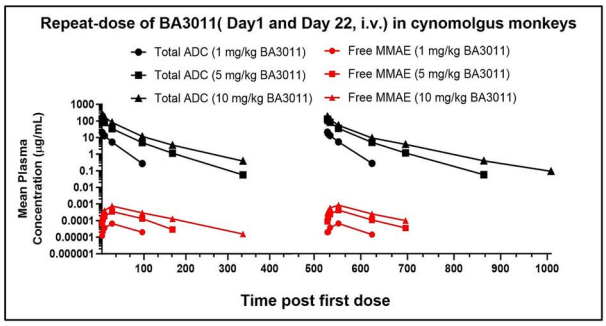


B

TK data in single-dose intravenous toxicity study in cynomolgus monkeys

| BA3011 Dose (mg/kg) | Analyte | $C_{max}$ (μg/mL) | $AUC_{0\text{-}t}$ (μg·h/mL) | $t_{1/2}$ (hr) |
|---|---|---|---|---|
| 1 | ADC | 24 | 443 | 16 |
| 3 | ADC | 70 | 1,825 | 38 |
| 10 | ADC | 241 | 7,120 | 46 |
| 1 | Total Ab | 22 | 492 | 31 |
| 3 | Total Ab | 66 | 2,095 | 55 |
| 10 | Total Ab | 209 | 8,485 | 65 |
| 1 | Intact Ab | 22 | 504 | 28 |
| 3 | Intact Ab | 73 | 2,220 | 50 |
| 10 | Intact Ab | 234 | 8,845 | 57 |
| 1 | Free MMAE | $4.6x10^{-5}$ | $2.4x10^{-3}$ | NC |
| 3 | Free MMAE | $3.0x10^{-4}$ | $1.5x10^{-2}$ | 39 |
| 10 | Free MMAE | $6.6x10^{-4}$ | $8.3x10^{-2}$ | 60 |

D

TK data of BA3011in repeat-dose intravenous toxicity study in cynomolgus monkeys

| TK Parameter | $C_{max}$ (μg/mL) | | $AUC_{0\text{-}t}$ (μg·h/mL) | | $t_{1/2}$ (hr) | |
|---|---|---|---|---|---|---|
| BA3011 Dose (mg/kg) | Day 1 | Day 22 | Day 1 | Day 22 | Day 1 | Day 22 |
| 1 | 20 | 19 | 381 | 379 | 17 | 19 |
| 5 | 122 | 103 | 2,920 | 2,330 | 37 | 38 |
| 10 | 242 | 186 | 6,710 | 4,780 | 43 | 48 |

Figure 6. Pharmacokinetic and toxicokinetic analysis of BA3011 in NHPs. (A) PK analysis for a single dose of BA3011 in cynomolgus monkeys. Plasma concentrations of total ADC, total antibody, and free MMAE in the serum of cynomolgus monkeys after a single dose of 3 mg/kg BA3011 (A) or repeat dosing on day 1 and day 22 with 1, 5, or 10 mg/kg (C) were determined at different times post dosing. TK parameters for single dose are summarized in (B) and for repeat dosing in (D).

assay. The binding site of BA301 was mapped using human/mouse chimeric AXL molecules. The data indicate that BA301 binds to a conformational epitope consisting of residues on both Ig-like domains of the AXL extracellular domain. When the binding kinetics of BA3011 were analyzed by SPR, we found that from pH 6.0 to pH 7.4, there was a simultaneous decrease in both affinity and maximum signal, similar to other CABs previously reported [22, 23]. By flow cytometry, BA3011 demonstrated strong binding to various human cancer cell lines at acidic pH, but very little binding under normal physiologic alkaline conditions.

BA3011 demonstrated *in vitro* anticancer activity in a pH-dependent manner. Greater cell-growth inhibition by BA3011 was found in a prostate cancer cell line (DU145) and a NSCLC cell line (LCLC-103H) in lower pH culture conditions. The conjugated isotype with no target binding was used as a negative control when evaluating the target-specific cell-killing activity of BA3011. Although limited activity of the isotype ADC was observed, confirming the cytotoxicity of BA3011 is antigen-dependent, there was detectable cell growth inhibition at the highest concentrations, which is probably caused by an unspecified mechanism and independent of the target [37, 38].

BA3011 was also tested in CDX mouse models and exhibited dose-dependent antitumor activity *in vivo*. At different efficacious doses, BA3011 significantly inhibited the tumor growth of NSCLC and prostate cancer xenografts, with an associated durable antitumor efficacy. In all the studies described herein, the parental unconjugated antibody BA301 was included as a control for efficacy. The binding of unconjugated antibody to AXL did not show the antitumor activity in these tumor models.

The nonclinical safety profile of BA3011 has been characterized with single and repeat dose studies up to one-month in duration, including assessment of reversibility of toxicological effects. The primary target organs affected by BA3011 treatment included lymphoid depletion in the thymus, bone marrow, and spleen. These organ changes led to a dose-dependent decrease in white blood cell parameters including significant decreases in neutrophils. The effect on the hematopoietic system was completely reversible, as there were no remarkable findings after the one-month recovery period.

In an *in vitro* human tissue cross-reactivity study, BA3011 did not show binding to cellular membranes in the tissues examined. The nonclinical safety findings with BA3011 represent toxicities similar to those observed with other MMAE-containing ADCs. These toxicities are easily monitored, reversible, and represent a manageable and acceptable risk in the intended patient population. The nonclinical safety profile of BA3011 was adequately characterized to support progression into clinical trials in advanced cancer indications.

The current results clearly demonstrate that BA3011 represents a novel, potentially highly effective targeted agent for the treatment of cancer patients.

BA3011 (Mecbotamab vedotin) is currently in multiple Phase 2 clinical trials in several solid tissue tumor settings.

## Acknowledgments

We thank BioDuro-Sundia Discovery Biology Team for their valuable technical assistance and R&D support; M.S. and J.B. for critical reading of the manuscript; and Dr. L.L. Sharp for help with the design and support of the *in vivo* murine model studies and nonhuman primate studies.
We also thank E.W. for medical writing assistance.

## Author contributions

Hwai Wen Chang (Conceptualization [equal], Data curation [equal], Investigation [equal], Methodology [equal], Writing—original draft [equal], Writing—review & editing [equal]), Jing

Downloaded from https://academic.oup.com/abt/advance-article/doi/10.1093/abt/tbaf006/8110027 by guest on 17 April 2025

Wang (Investigation [equal], Visualization [equal], Writing—original draft [equal], Writing—review & editing [equal]), Haizhen Liu (Data curation [equal], Investigation [equal], Visualization [equal], Writing—original draft [equal], Writing—review & editing [equal]), Charles Xing (Data curation [equal], Formal analysis [equal], Investigation [equal], Visualization [equal], Writing—original draft [equal], Writing—review & editing [equal]), Jian Chen (Data curation [equal], Investigation [equal], Visualization [equal], Writing—original draft [equal], Writing—review & editing [equal]), Gerhard Frey (Conceptualization [equal], Formal analysis [equal], Visualization [equal], Writing—original draft [equal], Writing—review & editing [equal]), William J. Boyle (Formal analysis [equal], Investigation [equal], Writing—original draft [equal], Writing—review & editing [equal]), and Jay M. Short (Conceptualization [equal], Formal analysis [equal], Investigation [equal], Writing—review & editing [equal]).

## Supplementary data

Supplementary data is available at *ABT* Online.

## Conflict of interest

All authors are shareholders of BioAtla Inc., which owns intellectual property rights to CABs- and PaCS-related technology. H.W.C., G.F., and J.M.S. are inventors of relevant patents. J.M.S. serves as a Director of BioAtla.

## Funding

All research described in this report was funded by BioAtla Inc. All authors are employees of BioAtla.

## Data availability

The datasets used and/or analyzed during the current study are available from the corresponding authors on reasonable request.

## Ethics and consent statement

N/A.

## Animal research statement

All animal studies were approved by and performed in accordance with the Institutional Animal Care and Use Committee protocols at the following research facilities: Crown Biosciences (San Diego, USA) and WuXi AppTec (Suzhou, China).

## References

1. Aguilera TA, Giaccia AJ. Molecular pathways: oncologic pathways and their role in T-cell exclusion and immune evasion-a new role for the AXL receptor tyrosine kinase. *Clin Cancer Res* 2017;**23**:2928–33. https://doi.org/10.1158/1078-0432.CCR-17-0189.
2. Gjerdrum C, Tiron C, Hoiby T. *et al.* Axl is an essential epithelial-to-mesenchymal transition-induced regulator of breast cancer metastasis and patient survival. *Proc Natl Acad Sci U S A* 2010;**107**:1124–9. https://doi.org/10.1073/pnas.0909333107.
3. Axelrod H, Pienta KJ. Axl as a mediator of cellular growth and survival. *Oncotarget* 2014;**5**:8818–52. https://doi.org/10.18632/oncotarget.2422.
4. Paccez JD, Vogelsang M, Parker MI. *et al.* The receptor tyrosine kinase Axl in cancer: biological functions and therapeutic implications. *Int J Cancer* 2014;**134**:1024–33. https://doi.org/10.1002/ijc.28246.
5. Lemke G. Biology of the TAM receptors. *Cold Spring Harb Perspect Biol* 2013;**5**:a009076. https://doi.org/10.1101/cshperspect.a009076.
6. Gay CM, Balaji K, Byers LA. Giving AXL the axe: targeting AXL in human malignancy. *Br J Cancer* 2017;**116**:415–23. https://doi.org/10.1038/bjc.2016.428.
7. Schoumacher M, Burbridge M. Key roles of AXL and MER receptor tyrosine kinases in resistance to multiple anticancer therapies. *Curr Oncol Rep* 2017;**19**:19. https://doi.org/10.1007/s11912-017-0579-4.
8. Zhu C, Wei Y, Wei X. AXL receptor tyrosine kinase as a promising anti-cancer approach: functions, molecular mechanisms and clinical applications. *Mol Cancer* 2019;**18**:153. https://doi.org/10.1186/s12943-019-1090-3.
9. Morimoto K, Yamada T, Hirai S. *et al.* AXL signal mediates adaptive resistance to KRAS G12C inhibitors in KRAS G12C-mutant tumor cells. *Cancer Lett* 2024;**587**:216692. https://doi.org/10.1016/j.canlet.2024.216692.
10. Williams EA, Vegas I, El-Senduny FF. *et al.* Pan-cancer genomic analysis of AXL mutations reveals a novel, recurrent, functionally activating AXL W451C alteration specific to myxofibrosarcoma. *Am J Surg Pathol* 2024;**48**:699–707. https://doi.org/10.1097/PAS.0000000000002191.
11. Pei JP, Wang Y, Ma LP. *et al.* AXL antibody and AXL-ADC mediate antitumor efficacy via targeting AXL in tumor-intrinsic epithelial-mesenchymal transition and tumor-associated M2-like macrophage. *Acta Pharmacol Sin* 2023;**44**:1290–303. https://doi.org/10.1038/s41401-022-01047-6.
12. Hugo W, Zaretsky JM, Sun L. *et al.* Genomic and transcriptomic features of response to anti-PD-1 therapy in metastatic melanoma. *Cell* 2016;**165**:35–44. https://doi.org/10.1016/j.cell.2016.02.065.
13. Son HY, Jeong HK. Immune evasion mechanism and AXL. *Front Oncol* 2021;**11**:756225. https://doi.org/10.3389/fonc.2021.756225.
14. Bhalla S, Fattah FJ, Ahn C. *et al.* Phase 1 trial of bemcentinib (BGB324), a first-in-class, selective AXL inhibitor, with docetaxel in patients with previously treated advanced non-small cell lung cancer. *Lung Cancer* 2023;**182**:107291. https://doi.org/10.1016/j.lungcan.2023.107291.
15. Felip E, Brunsvig P, Vinolas N. *et al.* A phase II study of bemcentinib (BGB324), a first-in-class highly selective AXL inhibitor, with pembrolizumab in pts with advanced NSCLC: OS for stage I and preliminary stage II efficacy. *J Clin Oncol* 2019;**37**:9098. https://doi.org/10.1200/JCO.2019.37.15_suppl.9098.
16. Rashdan S, Williams JN, Currykosky P. *et al.* A phase 1/2 dose escalation and expansion study of bemcentinib (BGB324), a first-in-class, selective AXL inhibitor, with docetaxel in patients with previously treated non-squamous NSCLC. *J Clin Oncol* 2018;**36**:e21043–e. https://doi.org/10.1200/JCO.2018.36.15_suppl.e21043.
17. Khongorzul P, Ling CJ, Khan FU. *et al.* Antibody-drug conjugates: a comprehensive review. *Mol Cancer Res* 2020;**18**:3–19. https://doi.org/10.1158/1541-7786.MCR-19-0582.
18. Sievers EL, Senter PD. Antibody-drug conjugates in cancer therapy. *Annu Rev Med* 2013;**64**:15–29. https://doi.org/10.1146/annurev-med-050311-201823.
19. Bhalla S, Gerber DE. AXL inhibitors: status of clinical development. *Curr Oncol Rep* 2023;**25**:521–9. https://doi.org/10.1007/s11912-023-01392-7.

Downloaded from https://academic.oup.com/abt/advance-article/doi/10.1093/abt/tbaf006/8110027 by guest on 17 April 2025

20. Miao YR, Rankin EB, Giaccia AJ. Therapeutic targeting of the functionally elusive TAM receptor family. *Nat Rev Drug Discov* 2024;**23**:201–17. https://doi.org/10.1038/s41573-023-00846-8.
21. Feng Q, Bennett Z, Grichuk A. *et al.* Severely polarized extracellular acidity around tumour cells. *Nat Biomed Eng* 2024;**8**:787–799. https://doi.org/10.1038/s41551-024-01178-7.
22. Chang HW, Frey G, Liu H. *et al.* Generating tumor-selective conditionally active biologic anti-CTLA4 antibodies via protein-associated chemical switches. *Proc Natl Acad Sci USA* 2021;**118**:e2020606118. https://doi.org/10.1073/pnas.2020606118.
23. Frey G, Cugnetti APG, Liu H. *et al.* A novel conditional active biologic anti-EpCAM x anti-CD3 bispecific antibody with synergistic tumor selectivity for cancer immunotherapy. *MAbs* 2024;**16**:2322562. https://doi.org/10.1080/19420862.2024.2322562.
24. Dy G, Alexander M, Camidge DR. 83TiP a phase II study of mecbotamab vedotin (BA3011), a CAB-AXL-ADC, alone and in combination with nivolumab in adult patients with metastatic NSCLC who had prior disease progression on or are intolerant to a PD-1/L1, EGFR, or ALK inhibitor. *J Thorac Oncol* 2023;**18**:S88. https://doi.org/10.1016/S1556-0864(23)00337-4.
25. Pollack S, Conley AP, Tap WD. *et al.* 53O results from a phase II part I trial of mecbotamab vedotin (BA3011), a CAB-AXL-ADC, in patients with advanced refractory sarcoma. *ESMO Open* 2024;**9**:1–2. https://doi.org/10.1016/j.esmoop.2024.102443.
26. Hoff CO, Dal Lago EA, Siqueira JM. *et al.* First use of AXL targeting in metastatic, refractory, adenoid cystic carcinoma: a case report. *JCO Precis Oncol* 2024;**8**:e2300633. https://doi.org/10.1200/PO.23.00633.
27. Chen M, Chen C, Shen Z. *et al.* Extracellular pH is a biomarker enabling detection of breast cancer and liver cancer using CEST MRI. *Oncotarget* 2017;**8**:45759–67. https://doi.org/10.18632/oncotarget.17404.
28. Doronina SO, Toki BE, Torgov MY. *et al.* Development of potent monoclonal antibody auristatin conjugates for cancer therapy. *Nat Biotechnol* 2003;**21**:778–84. https://doi.org/10.1038/nbt832.
29. Zwick MB, Parren PW, Saphire EO. *et al.* Molecular features of the broadly neutralizing immunoglobulin G1 b12 required for recognition of human immunodeficiency virus type 1 gp120. *J Virol* 2003;**77**:5863–76. https://doi.org/10.1128/jvi.77.10.5863-5876.2003.
30. Sasaki T, Knyazev PG, Clout NJ. *et al.* Structural basis for Gas6-Axl signalling. *EMBO J* 2006;**25**:80–7. https://doi.org/10.1038/sj.emboj.7600912.
31. Lambert JM, Morris CQ. Antibody–drug conjugates (ADCs) for personalized treatment of solid Tumors: a review. *Adv Ther* 2017;**34**:1015–35. https://doi.org/10.1007/s12325-017-0519-6.
32. Goyette MA, Cote JF. AXL receptor tyrosine kinase as a promising therapeutic target directing multiple aspects of cancer progression and metastasis. *Cancers (Basel)* 2022;**14**:466. https://doi.org/10.3390/cancers14030466.
33. Tang Y, Zang H, Wen Q. *et al.* AXL in cancer: a modulator of drug resistance and therapeutic target. *J Exp Clin Cancer Res* 2023;**42**:148. https://doi.org/10.1186/s13046-023-02726-w.
34. Sang YB, Kim JH, Kim CG. *et al.* The development of AXL inhibitors in lung cancer: recent progress and challenges. *Front Oncol* 2022;**12**:811247. https://doi.org/10.3389/fonc.2022.811247.
35. Van Renterghem B, Wozniak A, Castro PG. *et al.* Enapotamab Vedotin, an AXL-specific antibody-drug conjugate, demonstrates antitumor efficacy in patient-derived xenograft models of soft tissue sarcoma. *Int J Mol Sci* 2022;**23**:7493. https://doi.org/10.3390/ijms23147493.
36. Zhou L, Lu Y, Liu W. *et al.* Drug conjugates for the treatment of lung cancer: from drug discovery to clinical practice. *Exp Hematol Oncol* 2024;**13**:26. https://doi.org/10.1186/s40164-024-00493-8.
37. Zhao H, Atkinson J, Gulesserian S. *et al.* Modulation of macropinocytosis-mediated internalization decreases ocular toxicity of antibody-drug conjugates. *Cancer Res* 2018;**78**:2115–26. https://doi.org/10.1158/0008-5472.CAN-17-3202.
38. Aoyama M, Tada M, Yokoo H. *et al.* Fcgamma receptor-dependent internalization and off-target cytotoxicity of antibody-drug conjugate aggregates. *Pharm Res* 2022;**39**:89–103. https://doi.org/10.1007/s11095-021-03158-x.


Downloaded from https://academic.oup.com/abt/advance-article/doi/10.1093/abt/tbaf006/8110027 by guest on 17 April 2025

© The Author(s) 2025. Published by Oxford University Press on behalf of Antibody Therapeutics. All rights reserved. For permissions, please e-mail: journals.permissions@oup.com.
*Antibody Therapeutics*, 2025, tbaf006
https://doi.org/10.1093/abt/tbaf006
Research Article